Structural investigations of Co/ZrO_2 discontinuous multilayers by x-ray absorption fine structure spectroscopy

2003 J. Phys.: Condens. Matter 15 7237

(http://iopscience.iop.org/0953-8984/15/43/008)

INSTITUTE OF PHYSICS PUBLISHING JOURNAL OF PHYSICS: CONDENSED MATTER

J. Phys.: Condens. Matter **15** (2003) 7237–7252 PII: S0953-8984(03)63657-X

Structural investigations of Co/ZrO_2 discontinuous multilayers by x-ray absorption fine structure spectroscopy

O Proux[1], J S Micha[2,8], J R Régnard[3,4], A Traverse[5], B Dieny[6], F Ernult[6], P Bayle-Guillemaud[3], J L Hazemann[7] and L Giacomoni[3]

[1] Laboratoire de Géophysique Interne et Techtonophysique, 1381, Rue de la Piscine-Domaine Universitaire-F-38400 Saint-Martin-d'Hères, France
[2] CEA-Grenoble/DRFMC UMR 5819 Laboratoire de Physico-Chimie Moléculaire, 17 Avenue des Martyrs, F-38054 Grenoble Cedex 9, France
[3] CEA-Grenoble/DRFMC/SP2M, 17 Avenue des Martyrs, F-38054 Grenoble Cedex 9, France
[4] Université Joseph Fourier, BP 53 X, F-38041 Grenoble Cedex, France
[5] Laboratoire pour l'Utilisation du Rayonnement Electromagnétique, Bâtiment 209A, BP 34 F-91898 Orsay Cedex, France
[6] CEA-Grenoble/DRFMC/SPINTEC, 17 Avenue des Martyrs, F-38054 Grenoble Cedex 9, France
[7] Laboratoire de Cristallographie, 25 Avenue des Martyrs, BP 166 F-38042 Grenoble Cedex 9, France

E-mail: jsmicha@cea.fr

Received 19 May 2003
Published 17 October 2003
Online at stacks.iop.org/JPhysCM/15/7237

Abstract

X-ray absorption spectroscopy (XAS) is used to probe the evolution of the local order around the cobalt atoms in Co/ZrO_2 discontinuous multilayers as a function of the nominal Co layer thickness. A decrease of the mean number of Co nearest neighbours around Co atoms is observed as the Co layer nominal thickness decreases. XAS analysis is made according to a justified simple model based on two possible Co sites referred to as metallic (cobalt coordinated) and oxide (oxygen coordinated) sites. XAS results are in agreement with the results obtained by other structural characterizations using transmission electron microscopy and by magnetic and transport measurements showing the morphological evolution of the Co layers from the discontinuous state (multilayer of Co nanoparticles embedded in the oxide) to the continuous one by increasing the Co nominal thickness.

(Some figures in this article are in colour only in the electronic version)

1. Introduction

The spin dependent tunnel effect has attracted great interest in the last seven years. Besides its fundamental aspect, the tunnel magnetoresistance (MR) of magnetic tunnel junctions (MTJ)

[8] Author to whom any correspondence should be addressed.

could be useful for applications, especially in magnetic random access memories [1–4]. As MTJ (two continuous ferromagnetic electrodes separated by an insulating layer), ferromagnetic nanoparticles embedded in an insulating matrix also exhibit tunnel MR but with a weaker amplitude [1, 5–7]. In order to obtain high MR sensitivity in metal/oxide systems, the ferromagnetic particles can be arranged to form discontinuous multilayers (DCM) [8, 9]. Compared to MTJ, DCM are easier to prepare by physical vapour deposition such as sputtering. Besides the intrinsic physical properties of the magnetic metal and of the oxide, the local atomic order at the metal–oxide interface has been shown to have a strong influence on the spin dependent tunnel mechanisms, in particular on the polarization rate of the tunnelling electrons [10, 11]. Dispersion of the metallic species into the insulating matrix may lead to a drastic change in the magnetic and electronic properties of the metal/oxide/metal device. Moreover, the relative orientation of the magnetic moments of neighbouring particles, which is modified by the applied magnetic field H, also determines the shape of the MR variation [12]. As a result, the variation of the magnetization and of the electrical resistance of the DCM with H is mostly governed by the morphology of the nanogranular metal–oxide layers.

This paper presents the results of the characterization of the local structure around the Co atoms and of the morphology of the Co layers in Co/ZrO_2 multilayers as a function of the nominal deposited metal thickness (λ) and deposition rate (v). We compare the results obtained by several techniques which are sensitive to different length scales, from 1 to a few tens of ångströms. The central technique of this study is x-ray absorption spectroscopy (XAS), which appears to be particularly suitable for such systems without long-range order and composed of nanometric particles [13]. X-ray absorption near edge structure (XANES) and extended x-ray absorption fine structure (EXAFS) investigations have been performed at the Co K-edge to probe the structural local environment of the Co atoms. A quantitative analysis of the EXAFS data allows the determination of the nature and the number of nearest atomic neighbours (NN) at distance R from the probed central Co atoms, and the so-called Debye–Waller (DW) factor, corresponding to the mean-square relative displacement of the R distribution. In this paper the sensitivity of the EXAFS signal to the morphology of this nanoscaled metallic layer is stressed. Moreover, the investigation of the pre-edge and XANES features provides information about the electronic structure of the Co atoms and the number that are located in metallic sites. Both structural and morphological results from XAS analyses are compared to those deduced from transmission electron microscopy (TEM) micrographs and transport and magnetic measurements.

2. Experimental details

2.1. DCM elaboration

Co/ZrO_2 multilayers were grown by alternative magnetron sputtering of two separate targets (Co and ZrO_2) on an Si wafer or a glass substrate maintained at room temperature (RT). The base pressure was 2×10^{-8} Torr and the argon pressure was 3×10^{-3} Torr during deposition. The ZrO_2 layer nominal thickness was fixed at 40 Å whereas λ was varied from 2 to 62 Å. The bottom and top layers were ZrO_2 in order to (i) eliminate the possible interaction between the substrate and the Co aggregates; and (ii) protect the Co aggregates from oxidation by contact with air. The deposition of the [Co/ZrO_2] bilayer was repeated 40 times with either $v = 0.5$ or 0.9 Å s^{-1}. Specific ZrO_2 40 Å/Co λ/ZrO_2 40 Å trilayers were deposited with $\lambda = 8$ and 10 Å at $v = 0.5$ Å s^{-1} for TEM plane view observations.

2.2. Magnetic and transport measurements

The magnetic properties of the as-deposited Co/ZrO_2 multilayers ($v = 0.9$ Å s^{-1}) were measured at RT using a vibrating sample magnetometer. The magnetic field (H), up to 5 T, was applied in the plane of the Co layers. Resistance measurements were performed at 100 and 300 K in the current-in-plane (CIP) geometry for the DCM deposited at $v = 0.9$ Å s^{-1} [14].

2.3. XAS measurements

The XAS measurements were performed at the Laboratoire pour l'Utilisation du Rayonnement Electromagnétique (LURE, Orsay, France) D42 station and at the European Synchrotron Radiation Facility (ESRF, Grenoble, France) BM32 beamline respectively in the conversion electron yield (CEY) and in the fluorescence yield (FY) mode. Some samples were studied in both the CEY and the FY modes, and no substantial differences were observed in their corresponding spectra.

The CEY EXAFS measurements were carried out at RT or liquid nitrogen temperature [15], allowing in the latter case a good signal-to-noise ratio in an enlarged energy range due to the reduction of the dynamical part of the DW factor. Theoretical or semi-empirical models [16, 17] can be used in order to estimate the probing depth of this detection mode. Taking the bulk density values of ZrO_2 and Co (5.8 and 8.9 g cm^{-3} respectively), the probing depth is estimated to range between 600 and 700 Å in the λ-range covered. The probed thickness of the Co/ZrO_2 DCM then corresponds approximately to the 15 first top bilayers allowing the XAS signal relative to the Co atoms near the interface of the DCM and the SiO_2 substrate to be safely neglected. A (331) Si channel-cut monochromator was used in order to have an energy step of 0.5 eV in XANES part of the XAS spectra.

The FY measurements were carried out at RT using a 30 element solid germanium Canberra detector. The monochromator was a (111) Si 2-crystal. The dynamical bending of the second crystal permits a horizontal focusing of the beam without losing flux. The size of the x-ray spot was reduced to 0.3×0.3 mm^2 in order to increase the signal-to-noise ratio for DCM presenting a low Co mean concentration (low value of λ).

2.4. EXAFS analysis

EXAFS oscillations $\chi(k)$ were extracted from the raw data with the Autobk program [30] and simulations were performed using the *ab initio* backscattering phases and amplitudes calculated by the FEFF 6.01 code [31]. All the analyses were performed with k-weighted $\chi(k)$ signals whose Fourier transform (FT) correspond to the mean pseudo radial distribution function around Co atoms. The nearest peak from the origin is related to the photoelectron backscattering by Co or O neighbouring atoms. The inverse FT of this peak was fitted with FEFFIT to the FEFF-calculated and filtered signal $k\chi(k)$. To validate the analysis, a metallic Co foil reference spectrum was investigated in the same conditions.

3. Macroscopic characterization results

3.1. Transmission electron microscopy observations

Figure 1 shows TEM electron energy filtered images of two as-deposited Co/ZrO_2 trilayers for two Co nominal thicknesses $\lambda = 8$ and 10 Å obtained at the Co $L_{2,3}$ edge. Micrographs were digitized in order to quantify the morphology of the discontinuous layer and to estimate the in-plane Co coverage on ZrO_2. The in-plane views of the trilayers show that the Co layers

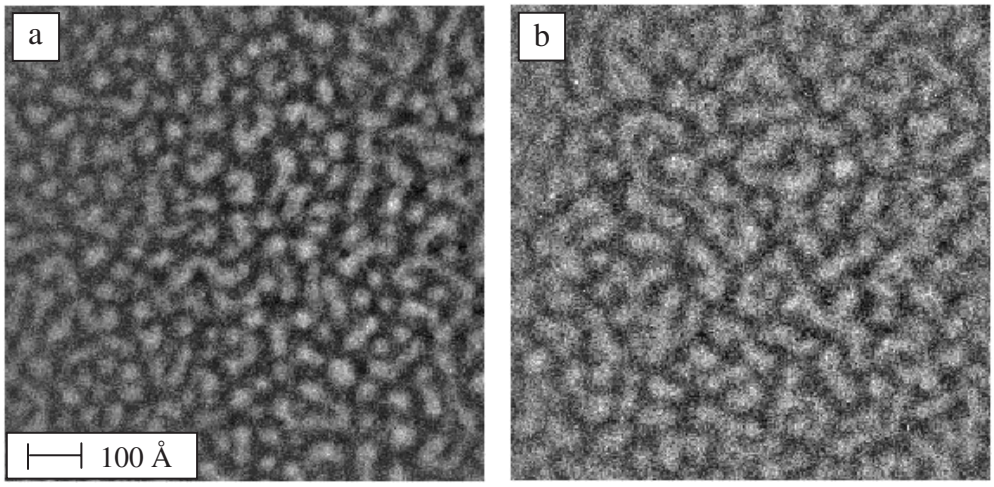

Figure 1. In-plane TEM electron energy filtered (Co edge) images of the as-deposited ZrO_2 40 Å/Co λ/ZrO_2 40 Å discontinuous trilayers ($v = 0.5$ Å s^{-1}) for (a) $\lambda = 8$ Å and (b) $\lambda = 10$ Å. The ZrO_2 matrix and Co particles are respectively of dark and light contrast.

(light contrast) form Co aggregates embedded in the ZrO_2 matrix (dark contrast). For $\lambda = 8$ Å, Co aggregates with radius $R_A \leqslant 25$ Å are almost spherical. Larger Co aggregates are also formed, with a chain-like shape; it is likely that they are due to the coalescence of spherical and smaller Co aggregates. By counting the fraction of white pixels the oxide coverage ratio is estimated to be about 40%. For $\lambda = 10$ Å, there are no longer small spherical Co aggregates but instead large ones formed by touching nanoparticles. The Co layer has a 2D coverage ratio of 55% and is close to the percolation threshold.

3.2. Transport properties

For $\lambda \leqslant 10$ Å, the CIP resistance is very large and decreases with the temperature (from about 10^7 Ω at 100 K to 2×10^6 Ω at 300 K). This non-metallic behaviour is due to the discontinuous nature of the Co layers: electrons cross the oxide barrier separating Co particles by the tunnel effect and thermally activated hopping [18, 19]. For larger thicknesses ($\lambda \geqslant 14$ Å), the CIP resistance falls to 10^2 Ω (100 K) and 2×10^2 Ω (300 K). It increases with temperature as in standard metals. Co layers are therefore continuous from the electrical point of view. The electric percolation threshold can be then located at $\lambda \simeq 11$ Å (for $v = 0.9$ Å s^{-1}).

3.3. Magnetic properties

The magnetization loops are shown in figure 2. For $\lambda = 6.3$ Å, the absence of hysteresis indicates that Co aggregates are superparamagnetic at RT. For $\lambda = 10.7$ Å, particles are clearly bigger due to the increase of initial susceptibility $(dM/dH)_{H=0}$. A slight hysteresis can be attributed to the non-spherical shape of the particles near the electric percolation threshold as suggested by the observation of a spin-glass-like behaviour at low temperature [14]. For $\lambda = 15.8$ Å, Co layers are continuous with a disordered soft ferromagnetic behaviour at RT.

Other results concern the saturation magnetization (M_S). Even for the largest λ DCM, M_S remains much smaller than the Co bulk saturation magnetization ($M_{S\,bulk} = 1445$ emu cm^{-3}). Two main effects explain this reduction. First, magnetic behaviour at the surface of the

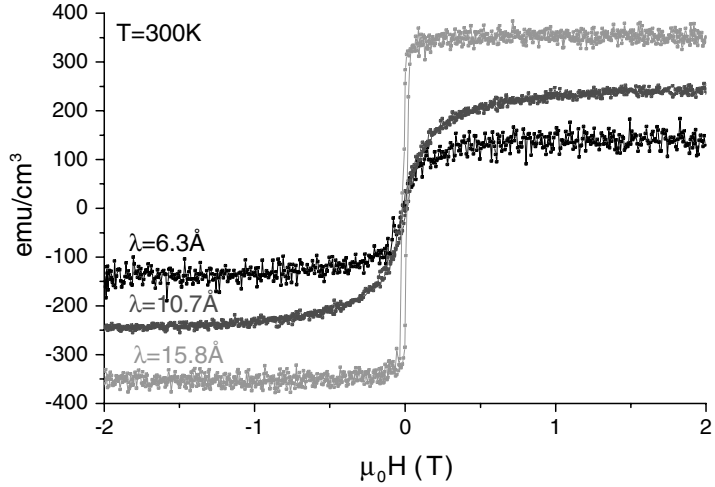

Figure 2. RT magnetization curves of as-deposited Co/ZrO_2 DCM grown at a deposition rate of 0.9 Å s^{-1}.

aggregates is different from that in the core. Canting and frustration of the surface spins may occur [20, 21]. They lead to a lack of complete saturation even at high field [22] and a decrease of the aggregate magnetization despite an enhancement of the magnetic moment per atom (MMA) observed in free aggregates [23, 24]. Secondly, due to the interactions with the atoms of the matrix, the electronic state of Co atoms not entirely surrounded by magnetic Co atoms may be modified as compared to the Co metallic ones [25]. It can be similar to that of Co ions. Co^{2+} and Co^{3+} are, for instance, paramagnetic and generally may be found in a low spin state [26]. They are far from being fully magnetized at RT even for high H-value. Exchange coupling between ferromagnetic Co atoms in the core and a disordered antiferromagnetic Co ions layer around them can also be present [27, 28].

The variation of M_S as a function of λ probably comes from the variation of the proportion of magnetic atoms. Following this idea, the proportion of Co atoms participating in the magnetism of the Co aggregates can be roughly estimated by assuming that they are either magnetic (with the full MMA as in bulk Co) or non-magnetic (in the ionic form without any effective magnetization). According to this most basic model, by taking the ratio $M_S/M_{S\,bulk}$, the magnetic fraction is found to be 7%, 15% and 24% for $\lambda = 6.3$, 10.7 and 15.8 Å respectively.

4. XAS results

4.1. XANES

The two series of DCM differing by the value of v exhibit the same evolution as a function of λ of their XANES spectra. Since the series relative to $v = 0.9$ Å s^{-1} has been measured with a higher energy resolution, the corresponding spectra are reported in figure 3. The normalised Co K-edge absorption spectra of DCM are superimposed on those of the CoO (2+ valence state), Co_3O_4 (both 2+ and 3+) and Co foil (metallic state) reference. The origin of the photoelectron energy is taken at the first inflection point of the Co foil spectrum. The spectra are normalised according to the height of the absorption jump at the edge given by the Autobk program.

The Co K-edge energy position is shifted to higher energy by increasing the valence state of the probed Co atoms (see the edge positions of the CoO and Co_3O_4 (arrow) spectra). The mean

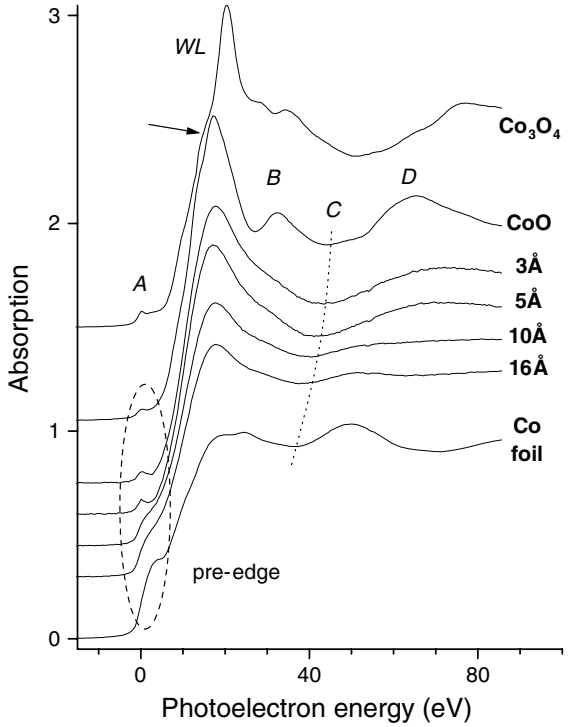

Figure 3. XANES spectra obtained at the Co K-edge of the as-deposited Co/ZrO_2 (CEY—300 K) DML grown at a deposition rate of 0.5 Å s^{-1}, compared with those of metallic Co foil, CoO and Co_3O_4. Spectra are shifted for clarity.

valence state of Co atoms in Co/ZrO_2 DCM is much closer to 2+ than 3+. Moreover, the peak located at the maximum of the absorption edge, the so-called white line (WL), is very marked for Co_3O_4. The fraction of Co atoms in DCM with the chemical neighbourhood of those in Co_3O_4 is then likely to be negligible as can be seen by the absence of a shoulder at the Co_3O_4 WL location in DCM spectra. In the following, DCM spectra will hence only be compared to the CoO spectrum relative to a single 2+ valence state.

The influence of the O and Co atomic shells around the central Co atoms on the XANES features has been previously studied in CoO ordered crystal [29]; the six nearest O atoms contribute to an enhancement of the height of the WL compared to that of metallic Co absorption spectrum; they also lead to the appearance of the pre-edge peak A, the bump B and the valley C; The further neighbours, 12 Co and 8 O, mostly sharpen the bump B and generate a large bump D.

For the as-deposited Co/ZrO_2 DCM, features B and D are very weak and the WL height is reduced. For $\lambda = 3$ and 5 Å the mean first neighbourhood composed of O atoms around the central Co atom is quite similar in the DCM to the arrangement of the first O layer in the CoO oxide but with a structural disorder. With the increase of λ from 5 to 10 and 16 Å, several variations occur: (i) the C valley shifts to lower energy (dotted curve), (ii) the weak and broad peak D, and the WL heights decrease, and (iii) a weak peak located at around 50 eV, and characteristic of the Co metal, appears on the DCM spectrum for $\lambda = 16$ Å. The DCM spectra seem then to be intermediate between those obtained for $\lambda = 3$ Å and bulk Co. Co atoms can be approximately regarded as located in two different groups of sites. The first

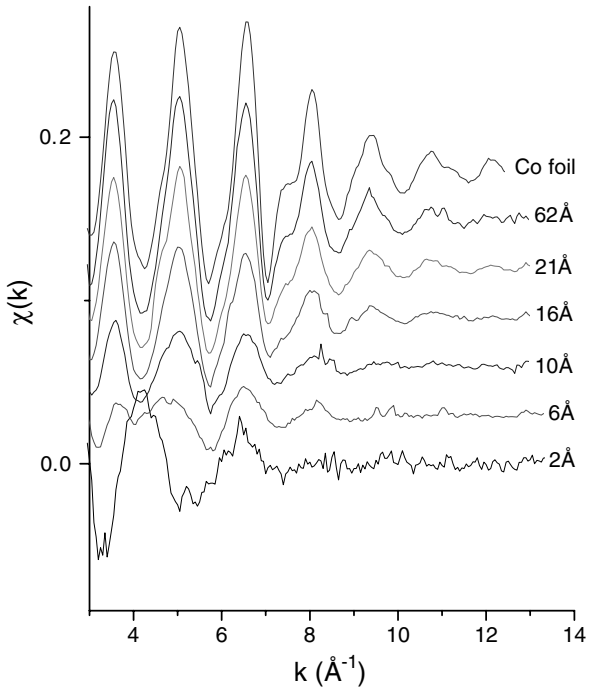

Figure 4. $\chi(k)$ EXAFS spectra obtained (FY—300 K) at the Co K-edge of the as-deposited Co/ZrO_2 DML ($v = 0.5$ Å s^{-1}) as a function of the Co layer nominal thickness and of the Co foil reference.

group corresponds to Co atoms with O neighbouring atoms without long-range order. The second group corresponds to Co atoms surrounded by Co atoms in a Co metal site. When λ increases, the fraction of the Co atoms present in such a Co metal site increases. Estimation of this metallic fraction will be presented in the discussion.

4.2. EXAFS qualitative analysis

In order to optimize the magnetoelectronic properties, the fraction of metallic Co atoms should be as high as possible. The DCM prepared at $v = 0.5$ Å s^{-1} have a higher Co metallic ratio than those prepared at $v = 0.9$ Å s^{-1} (not presented here).

Figure 4 shows the $\chi(k)$ EXAFS signal for the as-deposited Co/ZrO_2 DCM and for the Co foil reference. For small nominal thicknesses, the spectra display very weak oscillations due to a broad radial distribution of Co and O first neighbouring atoms around the Co central atoms and/or to the nanometric size of the probed aggregates. The $\lambda = 2$ Å EXAFS $k\chi(k)$ signal is mostly constituted of a single damped sinusoid similar to those observed in amorphous or ill-ordered materials. Due to the respective backscattering amplitude function of O atoms (the amplitude maximum occurs at low k-values) and Co atoms, $k\chi(k)$ oscillations correspond mostly to a highly disordered O shell. A large majority of the Co atoms then do not have a complete metallic environment. In the following discussion, these atoms will be referred as non-metallic atoms. They are located in an oxide-like site, even if this site does not obviously correspond in a strict manner to those existing in bulk Co oxides.

For $\lambda \geqslant 10$ Å, the $k\chi(k)$ spectra are quite similar to that of bulk Co. The amplitude of the oscillations clearly increases when λ increases. Most of the nearest neighbours around

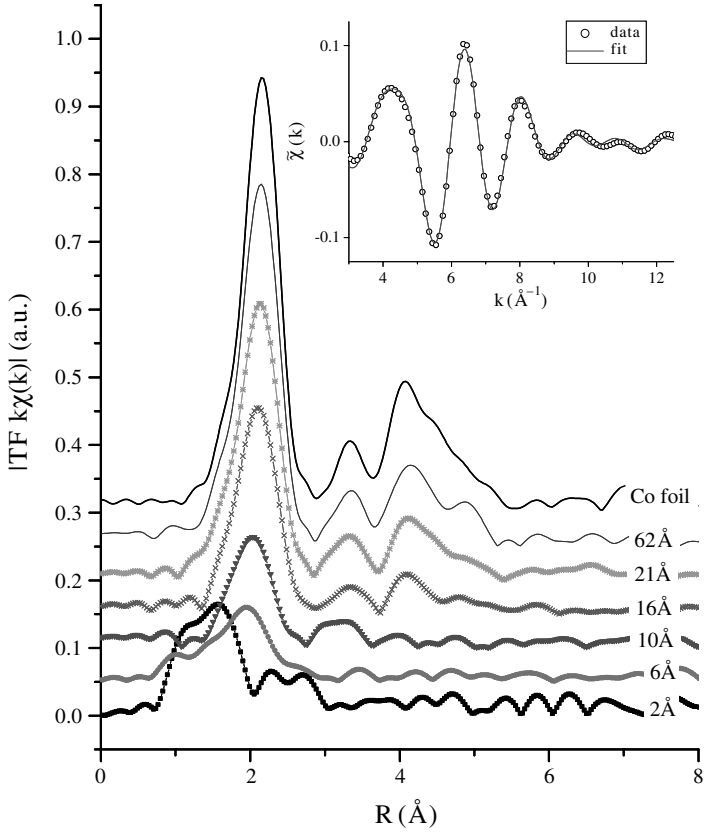

Figure 5. Moduli of the FT of the $k\chi(k)$ EXAFS spectra obtained (FY—300 K) at the Co K-edge from the as-deposited Co/ZrO_2 DCM ($v = 0.5$ Å s^{-1}) as a function of the Co layer nominal thickness. The spectrum corresponding to the largest Co layer thickness is similar to that of the Co foil. Inset: back FT (R-window from 1.1 to 2.8 Å) spectra of Co 10 Å/ZrO_2 (open circles) and the result of the fit (solid curve).

Co atoms are Co atoms. Corresponding DCM can be regarded as composed of Co atoms in a metallic environment. For the intermediate thickness $\lambda = 6$ Å, Co atoms can occupy both the metallic and 'oxide' sites.

These qualitative observations can be clarified with the help of the comparison of the k-weighted FT moduli (figure 5). Phase corrections have to be taken into account to obtain the real interatomic distances from the FT spectra abscissa. For $\lambda = 2$ Å, the FT modulus displays a broad peak centred around 1.8 Å (characteristic of the Co–O shell) and two small peaks centred around 2.1 and 2.4 Å. The last peak may be due to Co–Co and/or Co–Zr shells. Structural order is clearly very poor at radial distances larger than 3.5 Å. The small peaks at 4.2 Å and higher distance are attributed to the noise. For larger λ-values, the height of the peak located at a distance slightly shorter than the first Co–Co bond length measured in Co metal or [Co $\lambda = 62$ Å/ZrO_2]$_{40}$ DCM, increases with λ. For $\lambda = 10$ Å, the FT modulus is characteristic of a disordered Co metal environment. Increasing λ improves substantially the local order (giving rise to clear peaks at around 3.5 and 4 Å for $\lambda = 16$ Å). The apparent shift of the peak relative to the Co–Co bonds in DCM towards the distance corresponding to the first Co–Co bond in Co metal (2.48 Å) comes both from the decrease of the number of probed Co–O bonds and the increase of the number of probed Co–Co bonds.

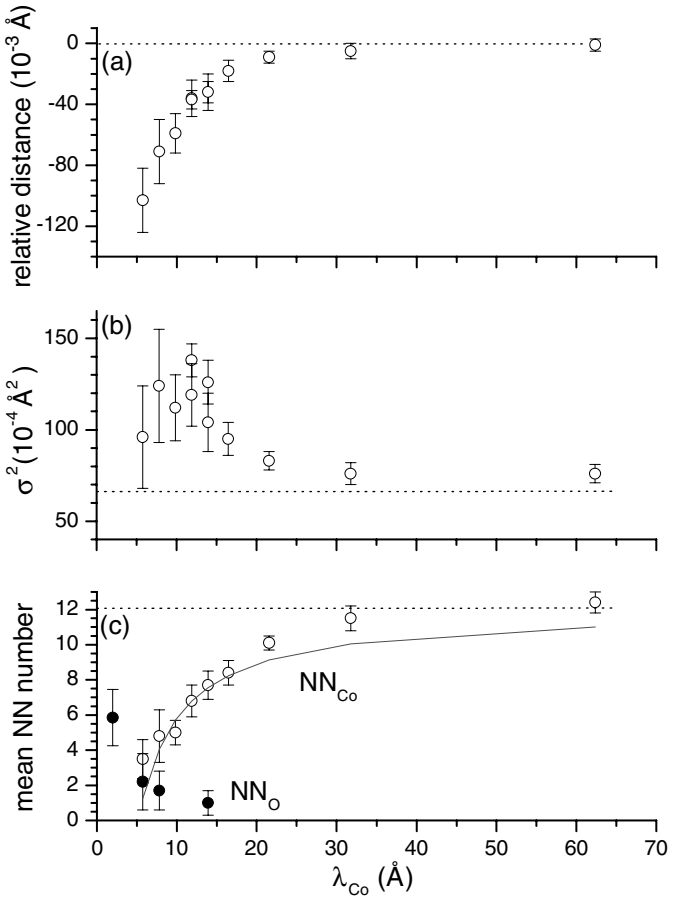

Figure 6. Results of the fits of the $k\chi(k)$ filtered signal obtained at the Co K-edge from the as-deposited Co/ZrO_2 DCM ($v = 0.5$ Å s^{-1}). (a) Mean first Co–Co distance, (b) Debye–Waller factor of the first shell Co, (c) mean nearest neighbours number of cobalt (open circles) and oxygen atoms (full circles). The dotted lines correspond to reference values deduced from the fit of the Co metallic foil spectra in the same conditions of analysis. The full curve is the plot of the model function according to the equation (4). Error bars are the statistical errors resulting from the fits.

4.3. EXAFS quantitative results

The values of the structural parameters (the first Co and O NN numbers, the Co–Co first distance and the corresponding DW factor) deduced from the fits of the $k\chi(k)$ signals are reported as a function of λ in figure 6. Two kinds of nearest atomic neighbourhood are used in the fits, depending on the value of λ. For $\lambda < 15$ Å, both O (characteristic of the first Co–O bond in the CoO reference) and Co (characteristic of Co–Co bond in metallic Co) first neighbours must be taken into account, whereas for larger λ only a single Co atoms shell is necessary.

- *Oxygen neighbourhood.* For $\lambda = 2$ Å, a single O shell is necessary for the simulation without any additional Co shell. The number of O nearest neighbours is quite similar to that of Co in the CoO structure. However, the quality of the fit remains poor due to the high disorder around the Co central atoms even by introducing an asymmetric radial

distribution (see the so-called cumulants method [35]). A more precise description of the oxygen neighbourhood around Co atoms would require EXAFS oscillations over a wider k-range. As a result, for higher λ-values, the number of nearest oxygen neighbours decreases with λ. This variation originates from the reduction of the fraction of probed central Co atoms with oxygen neighbours.

- *Co–Co first distance*. The Co–Co bond length is smaller than the Co–Co distance in Co metal ($R = 2.505$ Å): the bond length variation is negative for all the λ-values as reported in nanostructured aggregates due to the surface stress [33, 34]. The contraction tends towards 0 when λ increases and the mean first Co–Co bond length has apparently reached the reference value for $\lambda = 30$ Å. This variation can be explained by two complementary reasons. The first reason is the average effect over all the probed Co atoms: the fraction of Co atoms in bulk-like sites increases. The second reason comes from the absence of a model for the distribution of the first Co–Co distance. As the structural disorder and the width of the distribution decrease, the Gaussian distribution more accurately models the real distribution (see below).
- *Debye–Waller factor of the first Co–Co distance*. The value of the DW factor (σ^2), as λ increases, follows a general damping which is related to the increase of structural atomic ordering around an average Co central atom. The reduction of the mean local structural disorder around Co central atoms is attributed to a larger fraction of Co central atoms in well-ordered crystal sites. For the smallest values of λ, the structural disorder is so important that the harmonic distribution model of Co–Co first distance is not well adapted. The presence of the Co–O contribution in the same R-range cannot allow the extraction of the distance distribution or the application of the cumulants method. Finally, even for the thickest Co layers, one can note the remaining disorder (higher than that measured on a Co metallic foil).
- *Co NN number*. The number of Co nearest neighbours varies as a function of λ. This number tends towards 12 as λ increases, corresponding to the Co bulk value. It is a statistical average number calculated over all the central Co atoms. We shall discuss later how its variation with λ depends basically on the size of the particles and on the fraction of Co non-metallic sites.

5. Discussion

XAS analysis on Co/ZrO_2 at the Co K-edge gives a wealth of structural information about the local order around Co atoms. First, the presence of the oxygen atoms in the nearest vicinity of Co atoms is discussed. Secondly, an estimation of the number of this kind of Co atoms is proposed. Thirdly, at a greater length scale, a model of the variation of the number of Co nearest neighbours with respect to λ obtained by XAS is presented by taking into account the evolution of morphological parameters of the Co layers. Finally, information extracted from XAS measurements is inserted in the global structural and morphological diagram of Co/ZrO_2 multilayers as a function of λ.

5.1. Oxygen neighbours of Co atoms

For $\lambda \leqslant 5$ Å ($v = 0.5$ Å s^{-1}) and $\lambda \leqslant 10$ Å ($v = 0.9$ Å s^{-1}), XAS experiments indicate the presence of oxygen atoms in the Co nearest neighbourhood. According to XANES comparisons, most of the Co atoms surrounded by O atoms are likely to be in the 2+ valence state without excluding the 3+ valence state as in Co_3O_4 oxide. Local order around these non-metallic atoms is limited to very short distances: only the first O shell is clearly defined

and is similar to that of the first shell of the CoO oxide. However, with such poor local order, no long-range order structure as observed in CoO or Co_3O_4 oxides can be evidenced in the DCM by macroscopic techniques. The Co–O bonds are likely to be due to Co atoms (i) in substitution of Zr atoms in the sputtered ZrO_2 matrix or/and (ii) at the interface between Co aggregates and the ZrO_2 oxide matrix. Previous studies on Fe/ZrO_2 DCM grown using the same apparatus in similar conditions corroborate this conclusion [32].

5.2. Basic estimation of the Co metallic ratio

As the magnetic fraction was deduced from the variation of M_S with λ, so too the fraction of metallic Co atoms can be derived from the variation of the pre-edge features with λ. For small values of λ, the small pre-peak centred around 0 eV is at the same position as the pre-peak of the oxide references (figure 3). In contrast, for the higher nominal thickness, this edge feature seems to be intermediate between the Co metal and Co oxide features. Following the most simple assumption that Co atoms can be either in a metallic Co environment (metallic fraction F_{Co}) or surrounded by O atoms $(1 - F_{Co})$, F_{Co} can be roughly estimated with the help of the corresponding normalised pre-edge spectrum (normalised pre-edge absorption signal), S_{DCM}, expressed as a linear combination:

$$S_{DCM} = F_{Co}S_{Co} + (1 - F_{Co})S_{CoO} \tag{1}$$

where S_{Co} and S_{CoO} are the normalised pre-edge spectra of the Co metallic foil and CoO references respectively. Pre-edge features are preferred to those of XANES since they are not sensitive to structural disorder but to chemical environment. Reference signals, S_{Co} and S_{CoO}, were measured within the same run as the XAS experiments on DCM. Fits of the experimental edge spectra according to this model are satisfactory. All the results are gathered in figure 7 for the two series of DCM. For a given value of λ, the DCM deposited at $v = 0.5$ Å s^{-1} have a higher Co metallic ratio than those grown at $v = 0.9$ Å s^{-1} indicating that low deposition rate favours the formation of Co particles.

Previous Mössbauer spectroscopy and EXAFS experiments performed on Fe/ZrO_2 DCM with λ_{Fe} from 6 to 15 Å [32] have strongly suggested the presence of dead layers composed of non-metallic Fe atoms. Concerning the Co/ZrO_2 DCM, an equivalent Co thickness ($l_{Co–O}$) corresponding to Co atoms surrounded by O atoms can be assumed, which is constant with respect to λ but depends on v. When λ is lower than $l_{Co–O}$, all the Co atoms are assumed to be non-metallic with O neighbouring atoms ($F_{Co} = 0$). When λ exceeds $l_{Co–O}$, an equivalent $l_{Co–O}$ amount of Co is surrounded by O atoms whereas an equivalent $(\lambda - l_{Co–O})$ amount is in metallic Co sites. $l_{Co–O}$ can be seen as the total amount of non-metallic Co atoms roughly located on both sides of each nominally continuous Co layers. The F_{Co} ratio can then be simply written as

$$F_{Co} = \begin{cases} 0 & \text{for } l_{Co–O} \geqslant \lambda \\ \dfrac{\lambda - l_{Co–O}}{\lambda} & \text{for } l_{Co–O} \leqslant \lambda. \end{cases} \tag{2}$$

Comparisons of the experimental data with this model are shown in figure 7 (solid curves). The good agreement suggests that a constant amount of Co is surrounded by O atoms in these Co/ZrO_2 DCM. These atoms can be considered as dead or lost for the MR properties since their magnetic and electronic properties differ from those of metallic Co atoms in a ferromagnetic and metallic crystal. The $l_{Co–O}$ thickness is found to be around 2.5 and 6 Å for $v = 0.5$ and 0.9 Å s^{-1} respectively. The greater value of $l_{Co–O}$ found for the higher deposition rate is likely to be related to the better activation of the atomic interdiffusion between the oxide and metallic layers and to the increase of structural disorder due to the higher number and energy

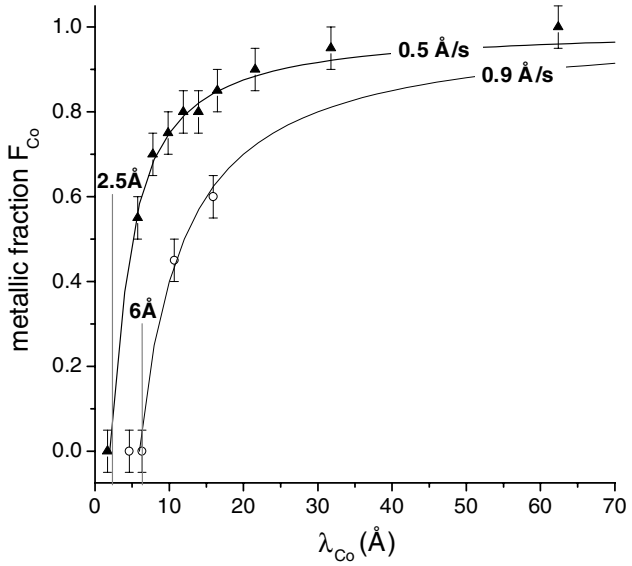

Figure 7. Estimation of the Co metallic ratio (F_{Co}) from the XANES signals versus the nominal thickness λ_{Co} of the DCM for two different deposition rates: $v = 0.5$ and 0.9 Å s^{-1} (symbols). Solid curves are Co metallic ratios calculated from equations (2) with $l_{Co–O} = 2.5$ and 6 Å.

of sputtered species impinging on the substrate. Since these mechanisms limit the aggregation process of the metallic element in ordered particles, $l_{Co–O}$-values can be regarded as a metallic 'aggregation threshold': for $\lambda < l_{Co–O}$, no substantial amount of metallic Co can be found in the ZrO_2 matrix. Finally, the Co magnetic ratios obtained from the saturation magnetization values are smaller than the Co metallic ratios obtained from the XANES adjustments. Numerous Co atoms with reduced magnetic moments, near or at the surface of Co aggregates with chain-like shape or composed of touching nanocrystallites, actually contribute to the underestimation of the magnetic Co atoms.

5.3. Co metallic aggregates

The Co NN number is lower for the Co/ZrO_2 DCM than for the bulk metallic Co reference (figure 6(c)). Two main parameters can govern this reduction: (i) the fraction of under-coordinated atoms at the surface of nanometric aggregates is not negligible, and (ii) Co atoms are roughly located in two different sites (pure Co aggregates and Co surrounded by O atoms). This repartition can be estimated from the F_{Co}-value (number of metallic Co with respect to the total number of Co atoms, see section 5.2). The measured Co NN number for the DCM must then be compared to the Co NN number of the reference weighted by F_{Co} to account for this repartition.

Numerous studies have established the correlation between the NN number reduction and the size of the aggregates [36–38]. However, these theoretical calculations are performed when atoms gather in a polyhedral aggregates. In this study, the Co aggregates evolve from a roughly spherical shape (below the electric percolation threshold) to larger chain-like particles (see figure 1). The Co layers in the DCM are discontinuous for low values of λ and continuous for higher ones.

One can estimate the resulting NN number when the metallic Co atoms are gathered in spherical aggregates or in continuous layers. Similar calculations can be found in previous

studies [39–41]. In the case of spherical particles, the mean NN number is expressed in good approximation as

$$\overline{N_{\text{sphere}}} = N_C F_{\text{Co}}\left(1 - \frac{3d}{4R_{\text{A}}}\right) \tag{3}$$

where R_{A} is the particle radius, F_{Co} the fraction of non-metallic Co atoms deduced in section 5.2, $N_C = 12$ (bulk Co NN number value) and d the first interatomic distance.

The mean particle size can hence be estimated from the EXAFS NN number in the DCM. However, there is a large discrepancy between the size estimated by EXAFS and those measured by TEM. On one hand, the energy filtered TEM is sensitive to heavily concentrated Co regions irrespective of the valence state of Co atoms and structural local order around them. The size obtained is of the order of a few tens of ångströms. On the other hand, EXAFS is mainly sensitive to well-ordered atomic structure: probed Co atoms surrounded by large distance distributed Co atomic neighbours do not fully contribute to the corresponding EXAFS shell signal amplitude. Moreover, the generally accepted uncertainty on the measured NN number is about 10–20% and the nanoparticles are not strictly identical and spherical. The estimation of the mean nanoparticle size from the absolute value of the mean EXAFS NN number (even corrected by F_{Co}) leads then to an approximate and very reduced size compared to that obtained by macroscopic techniques [41]. But the comparison of EXAFS NN numbers values can be safely exploited to obtain structural information.

In our case, we put in the model morphological parameters. We assume that the Co layers are composed of spherical aggregates (radius R_{A}) forming a 2D hexagonal lattice (distance Λ between the centres of two neighbouring aggregates). According to the Co deposited volume conservation,

$$\lambda - l_{\text{Co–O}} = \frac{8\pi}{\sqrt{3}}\frac{R_{\text{A}}^3}{\Lambda^2}.$$

Previous grazing incidence small-angle x-ray scattering (GISAXS) experiments performed on Co/SiO_2 DCM [42, 43] have suggested a proportional relationship between R_{A} and Λ: $\Lambda = \alpha R_{\text{A}}$. By following these descriptions the mean NN number is then

$$\overline{N_{\text{sphere}}} = N_C\left(1 - \frac{l_{\text{Co-O}}}{\lambda}\right)\left(1 - \frac{d}{\lambda - l_{\text{Co–O}}}\frac{2\pi\sqrt{3}}{\alpha^2}\right). \tag{4}$$

Calculations have been performed from equations (4) with the following numerical values: $d = 2.505$ Å (Co–Co distance in bulk Co), $l_{\text{Co–O}} = 2.5$ Å (as determined in section 5.2) and $\alpha = 3.2$ fixed after [42]. The results obtained are shown as a solid curve in figure (6(c)) for comparison with the experimental data (open circles).

Two regions can be defined. For $\lambda \leqslant 16$ Å, the experimental values are found to be in agreement with the simulated data. For $\lambda > 20$ Å, the previous model based on specific particle size, shape and organisation is no longer valid. EXAFS results hence agree with the morphological evolution of the Co layers from a discontinuous (Co aggregates) to a continuous layer.

5.4. Co/ZrO_2 DCM morphology diagram

The results concerning the morphology of the Co layers are summarised in figure 8. Three frontiers are reported.

(i) The Co aggregation threshold deduced from the XANES investigation and magnetic measurements, estimated to about 2.5 Å. This value is significant of the amount of both non-metallic and non-magnetic Co atoms having neighbouring O atoms.

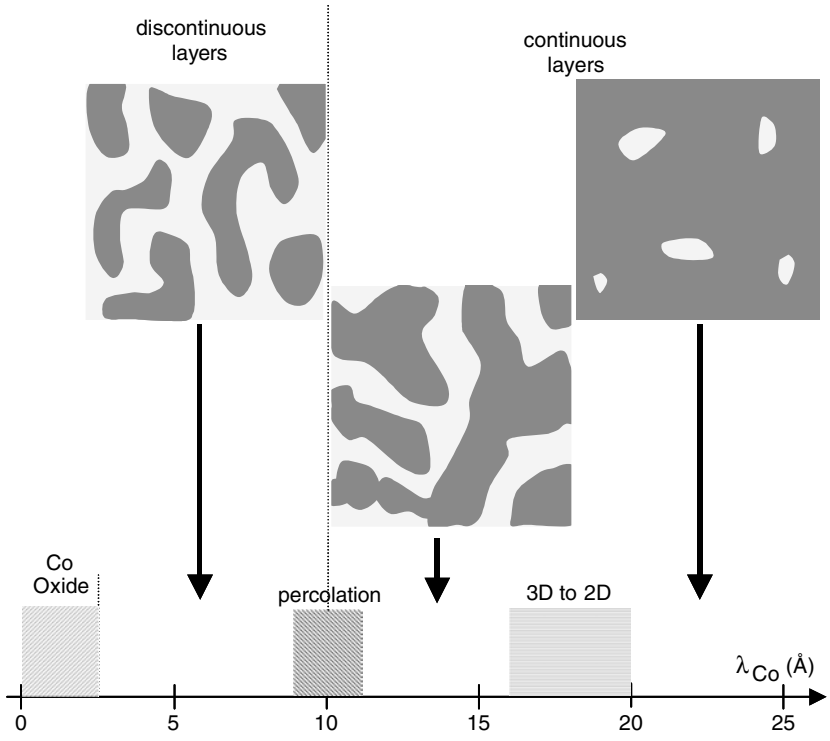

Figure 8. Schematic representation of the structural evolution of the Co layers in the Co/ZrO_2 DCM ($v = 0.5$ Å s^{-1}). The ZrO_2 matrix and Co particles are respectively in light and dark contrast.

(ii) From TEM micrographs and transport measurements, the electrical percolation threshold has been estimated to about 10 Å.

(iii) A 3D–2D transition region has been defined by EXAFS between 16 and 20 Å corresponding to the transition from a discontinuous (surface to volume ratio characteristic of 3D aggregates i.e. with a rather spherical shape) to a continuous layer (surface to volume ratio characteristic of 2D layer i.e. continuous or composed of rather pancake and chain-like particles).

The percolation threshold is obviously not evidenced by the measurement of the EXAFS mean NN number.

The positions of the three thresholds are highly dependent on the difference of the surface energy between the metal and the insulator matrix as well as on the substrate temperature during the deposition. For multilayers grown by sputtering at RT, it has been observed for small values of λ that Co does not wet SiO_2 [9, 42] and Al_2O_3 layers [44]: the electrical percolation threshold was found to be around 20 Å and between 15 and 20 Å respectively. These ranges are slightly higher than that measured in Co/ZrO_2 DCM. The reduced λ-range for preparing DCM by sputtering with Co and ZrO_2 limits then the optimisation of the MR properties as a function of λ. Grazing incidence small-angle scattering data are under analysis to determine the growth process in this metal–oxide system.

6. Conclusion

The structure of Co/ZrO_2 multilayers grown with two Co atoms deposition rates (v) has been studied. Macroscopic measurements have clearly established the discontinuity of the metallic layer for a Co nominal deposited layer thickness (λ) lower than 10 Å. A reduction of the saturation magnetization in DCM with respect to the bulk Co value is observed. Moreover, the XAS indicates that the mean number of Co nearest neighbours around Co atoms is lower than that in bulk Co due to the finite size of the layer. The evolution of this number with λ is governed by the variation of the fraction of Co atoms having an oxygen atom as a first neighbour and the size of the particles composing the layer. According to a basic model, the number of Co atoms with oxygen neighbours which are lost for the MR properties can be estimated to an equivalent deposited thickness of 2.5 Å ($v = 0.5$ Å s^{-1}) and 6 Å ($v = 0.9$ Å s^{-1}) for any value of λ. The electronic state of the non-metallic Co atoms probed by XANES is rather similar to that of Co^{2+} ions in CoO but the local order around them is limited to the first O shell.

Three thresholds have been found: aggregation, percolation and 2D–3D layers thresholds. Their location has allowed the determination of the λ-range corresponding to the presence of Co particles with a negligible fraction of non-magnetic and non-metallic Co atoms. In addition to the structural disorder, this result represents an argument to explain the reduced efficiency of the spin-polarized transport in DCM compared to that predicted by theoretical calculations.

The quantitative analysis of the XANES experiments is now in progress, in order to determine accurately the local structure and the oxidation state of Co in the various DCM. Grazing incidence x-ray diffraction and GISAXS data are under analysis in order to complete the structural and the morphological study of Co/ZrO_2 DCM.

References

[1] Gittleman J I, Goldstein Y and Bozowski S 1972 *Phys. Rev.* B **5** 3609
[2] Jullière M 1975 *Phys. Lett.* A **54** 225
[3] Moodera J S, Kinder L R, Wong T M and Meservey R 1995 *Phys. Rev. Lett.* **74** 3273
[4] Miyazaki T and Tezuka N 1995 *J. Magn. Magn. Mater.* **139** L231
[5] Milner A, Gerber A, Groisman B, Karpovsky M and Gladkikh A 1996 *Phys. Rev. Lett.* **76** 475
[6] Honda S, Okada T, Nawate M and Tokumoto M 1997 *Phys. Rev.* B **56** 14566
[7] Gerber A, Milner A, Groisman B, Karpovsky M and Gladkikh A 1997 *Phys. Rev.* B **55** 6446
[8] Sankar S, Dieny B and Berkowitz A E 1997 *J. Appl. Phys.* **81** 5512 and reference therein
[9] Dieny B, Sankar S, McCartney M R, Smith D J, Bayle-Guillemaud P and Berkowitz A E 1998 *J. Magn. Magn. Mater.* **185** 283
[10] De Boer P K, de Wijs G A and de Groot R A 1998 *Phys. Rev.* B **58** 15422
[11] De Teresa J M, Barthélémy A, Fert A, Contour J P, Montaigne F and Seneor P 1999 *Science* **286** 507
[12] Inoue J and Maekawa S 1996 *Phys. Rev.* B **53** R11927
[13] Traverse A 1998 *New J. Chem.* **22** 677
[14] Giacomoni L 1998 *PhD Thesis* Université Joseph Fourier, Grenoble 1, France
[15] Mimault J, Faix J J, Girardeau T, Jaouen M and Tourillon G 1994 *Meas. Sci. Technol.* **5** 482
[16] Girardeau T, Mimault J, Jaouen M, Chartier P and Tourillon G 1992 *Phys. Rev.* B **46** 7144
[17] Schroeder S L M 1996 *Solid State Commun.* **98** 405
[18] Sheng P, Abeles B and Arie Y 1973 *Phys. Rev. Lett.* **31** 44
[19] Abeles B, Sheng P, Coutts M D and Arie Y 1975 *Adv. Phys.* **24** 407
[20] Coey J M D 1971 *Phys. Rev. Lett.* **27** 1140
[21] Vargas P, d'Albuquerque e Castro J and Altbir D 1999 *Phys. Rev.* B **60** 6541
[22] Respaud M, Broto J M, Rakoto H, Fert A R, Thomas L, Barbara B, Verelst M, Snoeck E, Lecante P, Mosset A, Osuna J, Ould Ely T, Amiens C and Chaudret B 1998 *Phys. Rev.* B **57** 2925
[23] Billas I M L, Becker J A, Châtelain A and de Heer W A 1993 *Phys. Rev. Lett.* **71** 4067
[24] Billas I M L, Châtelain A and de Heer W A 1994 *Science* **265** 1682

[25] Zanghi D, Teodorescu C M, Petroff F, Fischer H, Bellouard C, Clerc C, Pélissier C and Traverse A 2001 *J. Appl. Phys.* **90** 6367
[26] Cox P A 1992 *Transition Metal Oxides. An Introduction to their Electronic Structure and Properties* (Oxford: Clarendon)
[27] Meiklejohn W H and Bean C P 1956 *Phys. Rev.* **102** 1413
[28] Morrish A H and Haneda K 1983 *J. Magn. Magn. Mater.* **35** 105
[29] Jiang T and Ellis D E 1996 *J. Mater. Res.* **11** 2242
[30] Newville M, Livins P, Yacoby Y, Rehr J J and Stern E A 1993 *Phys. Rev.* B **47** 14126
[31] Mustre de Leon J, Rehr J J and Zabinsky S I 1991 *Phys. Rev.* B **44** 4146
[32] Auric P, Micha J S, Proux O, Giacomoni L and Régnard J R 2000 *J. Magn. Magn. Mater.* **217** 175
[33] Apai G, Hamilton J F, Stohr J and Thompson A 1979 *Phys. Rev. Lett.* **43** 165
[34] Balerna A, Bernieri E, Reale A, Santucci S, Burattini E and Mobilio S 1985 *Phys. Rev.* B **31** 5058
[35] Bunker G 1983 *Nucl. Instrum. Methods Phys. Res.* **207** 437
[36] MacKay A L 1962 *Acta Crystallogr.* **15** 916
[37] Fritsche H G and Benfield R E 1993 *Z. Phys.* D **26** 15
[38] Khoutami A, Legrand B, Mottet C and Tréglia G 1994 *Surf. Sci.* **307–309** 735
[39] Borowski M 1997 *J. Physique Coll.* IV **2** C 259
[40] Proux O, Mimault J, Revenant-Brizard C, Régnard J R and Mevel B 1999 *J. Phys.: Condens. Matter* **11** 147–62
[41] Proux O, Régnard J R, Manzini I, Revenant-Brizard C, Rodmacq B and Mimault J 2000 *Eur. Phys. J.* D **9** 115
[42] Thiaudière D, Proux O, Micha J S, Revenant C, Régnard J R and Lequien S 2000 *Physica* B **283** 114
[43] Naudon A, Babonneau D, Petroff F and Vaurès A 1998 *Thin Solid Films* **319** 81
[44] Briático J, Maurice J L, Carrey J, Imhoff D, Petroff F and Vaurès A 1999 *Eur. Phys J.* D **9** 517